AIAA 96-2386
Study of Semi-Span Model Testing Techniques

G. M. Gatlin and R. J. McGhee
NASA Langley Research Center
Hampton, VA 23681-0001

14th Applied Aerodynamics Conference
June 17-20, 1996 / New Orleans, LA

STUDY OF SEMI-SPAN MODEL TESTING TECHNIQUES

Gregory M. Gatlin*
and
Robert J. McGhee†
NASA Langley Research Center
Hampton, VA

Abstract

An investigation has been conducted in the NASA Langley 14- by 22-Foot Subsonic Tunnel in order to further the development of semi-span testing capabilities. A twin engine, energy efficient transport (EET) model with a four-element wing in a takeoff configuration was used for this investigation. Initially a full span configuration was tested and force and moment data, wing and fuselage surface pressure data, and fuselage boundary layer measurements were obtained as a baseline data set. The semi-span configurations were then mounted on the wind tunnel floor, and the effects of fuselage standoff height and shape as well as the effects of the tunnel floor boundary-layer height were investigated. The effectiveness of tangential blowing at the standoff/floor juncture as an active boundary-layer control technique was also studied. Results indicate that the semi-span configuration was more sensitive to variations in standoff height than to variations in floor boundary-layer height. A standoff height equivalent to 30 percent of the fuselage radius resulted in better correlation with full span data than no standoff or the larger standoff configurations investigated. Undercut standoff leading edges or the use of tangential blowing in the standoff/floor juncture improved correlation of semi-span data with full span data in the region of maximum lift coefficient.

Introduction

Generally in most types of wind tunnel testing, research requirements dictate that the most accurate data be obtained and that the correct flight conditions be simulated. These issues are increasingly important in order to develop accurate performance characteristics particularly at the low-speed takeoff and approach conditions encountered by subsonic transport aircraft. Typically the Reynolds numbers achievable at the speeds appropriate for takeoff and approach conditions in the current facilities available are below the desired full-scale Reynolds number. This need to extend Reynolds number testing capabilities up to full-scale conditions can be satisfied with the development of a semi-span testing capability. This testing technique has been suggested as a tool which should be developed to provide state-of-the-art wind tunnel research capabilities[1,2].

Semi-span testing offers several advantages over full span testing. Due to the larger model size provided by semi-span testing, not only is the desired increased Reynolds number testing capability produced, but the larger model size also improves data quality due to improved model strength, stiffness, and overall fidelity. Constructing only half the model yields further benefits in terms of reduced model cost. The complex high-lift systems and any wing mounted propulsion simulation systems will only need to be produced for one wing. Another advantage of semi-span testing is the absence of sting-support interference effects.

Semi-span testing however, is not free from any drawbacks. These include increased wind-tunnel wall interference effects due to increased model size, and the effects of semi-span model mounting. One of the most significant challenges is how to remove the effects of the tunnel wall boundary layer on the flow over the semi-span model. These adverse effects include loss of model symmetry, wall boundary layer separation, and formation of vortical flow in the juncture regions. Research previously conducted[3] indicates that even when the wall boundary layer remains attached, it can still substantially influence the flow over the semi-span model. One technique which has been investigated to isolate the effects of the wall boundary layer is to mount the semi-span model on a splitter plate which is offset from the tunnel wall outside the wall boundary layer. This technique certainly eliminates any wall boundary layer effects; however, it introduces difficulties in maintaining a uniform flow over the model without

*Research Scientist, Aerodynamics Division. Senior Member AIAA.

†Research Scientist, Aerodynamics Division.

introducing any undesirable flow angularity. These issues can be overcome, but generally at the expense of a substantial calibration effort[4]. Results from previous semi-span testing technique studies have generally been more promising when a non-metric boundary layer standoff is used between the semi-span model and the wind tunnel wall[4,5,6].

In order to further understand the flow physics involved in semi-span testing as well as to develop techniques by which to eliminate or minimize the effects of the wall boundary layer, both computational methods[7] and experimental studies have been utilized. A wind tunnel investigation has been conducted in the NASA Langley 14- by 22-Foot Subsonic Tunnel using both a full span and a semi-span transport model with a four-element wing in a take-off configuration. The full span configuration was tested initially and force and moment data, wing and fuselage surface pressure data, and fuselage boundary layer measurements were obtained as a baseline data set. The semi-span configurations, which were designed to use a floor mount and a non-metric boundary layer standoff, were then tested to study the effects of standoff height and shape as well as the effects of the tunnel floor boundary layer height. The effectiveness of tangential blowing as an active boundary-layer control technique was also studied. It is the results of these investigations which will be presented in this paper.

Nomenclature

b	wing span, in
BL	boundary layer
BLRS	boundary layer removal system
C_D	drag coefficient
C_L	lift coefficient
C_M	pitching-moment coefficient
C_p	pressure coefficient
C_μ	blowing coefficient, per blowing jet
d	fuselage diameter, in
M	Mach number
R_n	Reynolds number based on mean geometric chord
y	spanwise location
x/c	longitudinal distance from airfoil leading edge nondimensionalized by local wing chord
x/L	longitudinal distance from fuselage nose nondimensionalized by fuselage length
u/u_∞	velocity measured from fuselage boundary layer rake nondimensionalized by freestream velocity
z	height above fuselage surface, in
α	angle of attack, deg
2-D	two dimensional
3-D	three dimensional

Test Facility and Model Description

The investigation was conducted in the Langley 14- by 22-Foot Subsonic Tunnel[8]. This facility is a closed-circuit, single-return, atmospheric wind tunnel capable of producing a maximum speed of 338 feet per second. A floor boundary layer removal system is located at the entrance to the test section and was used in the current investigation to study the effects of variations in floor boundary layer height on the semi-span configuration.

The model used in the investigation was a 10.59 foot span, unpowered, twin engine transport known as the energy efficient transport (EET) configuration. The full span model, as shown in figure 1, was tested first in order to provide a baseline database. The fuselage was 9.91 feet long and had a maximum diameter of 13.8 inches. The wing employed a supercritical airfoil with a four-element flap system consisting of a slat, main element, vane, and flap. All of the results presented in this paper are for a takeoff configuration with the slats deflected -50°, the vanes 15°, and the flaps 30°. These deflection angles are all with respect to the main wing element. Pressure instrumentation was located on the wing and fuselage as illustrated in figure 1. The full span model was mounted on a six-component strain-gage balance and supported by a sting which entered the lower aft end of the fuselage. No vertical or horizontal tails were used in the investigation.

The semi-span model consisted of the port wing from the full span model and a semi-fuselage which was fabricated from a mold of the full-span fuselage. In addition, all semi-span configurations were tested with a simulated sting. These steps were taken to ensure no geometric differences would exist between the full span and semi-span configurations. A photograph of the semi-span model installation in the wind tunnel is presented in figure 2. The model was mounted on a 15.75 foot diameter turntable on the floor of the tunnel approximately six feet aft of the tunnel floor boundary layer removal system (BLRS). A six-component strain-gage balance was used to measure forces and moments on the wing and semi-fuselage. All standoffs however,

were non-metric. A polyurethane foam seal was used around the perimeter of the fuselage to fill the 0.25-inch gap between the fuselage and the standoff so that no freestream flow would enter this region. This seal was carefully installed during each standoff installation to ensure that no fouling would occur between the metric fuselage and the non-metric standoffs. All standoffs were attached to the tunnel floor and sealed such that no freestream flow could pass between the standoff and the floor. The semi-span model was tested with no standoff, and 2-inch and 6.4-inch 2-D standoffs. These standoffs were the same shape as the perimeter centerline shape of the fuselage. Additionally, a 3-D 6.4-inch standoff which was a mirror image of the semi-fuselage, and a complete right side of the fuselage were tested. All of these standoff shapes are presented in figure 3. Further tests were conducted in which three-dimensionally shaped undercut leading edges were tested on the 2-inch standoff configuration. Illustrations of these undercut leading edges are presented in figure 3(b). Another testing technique investigated was to reenergize the floor boundary layer through the use of tangential blowing in the juncture between the standoff and the tunnel floor. Ten jets, five on top and five below the model, were placed on the floor and oriented to blow tangent to the local standoff surface. Each jet was produced by a 0.25-inch diameter tube and was set to $C_\mu = 0.003$. A sketch illustrating the details of the tangential blowing technique is presented in figure 4.

Test Conditions and Techniques

All testing for both the full span and semi-span configurations was conducted at $M = 0.20$, $R_n = 1.6$ million, and over an angle-of-attack range of -4° to 24°. The moment reference center was located on the fuselage centerline 64.70 inches back from the nose on both the full span and semi-span configurations. Transition grit was placed on the fuselage nose and on the nacelles, but not on any of the wing elements for both configurations. Base pressure corrections were applied to the full span configuration to account for the effects of the sting entering the lower aft end of the fuselage. A simulated sting was positioned external to the semi-span configuration so as to generate the same flowfield encountered by the full span configuration. Since the simulated sting did not enter the semi-span fuselage, no base pressure corrections were applied. A simulated semi-sting was used for the no standoff and 2-inch standoff configurations (see figure 2). A simulated full sting was used for all configurations with a larger standoff. For all semi-span configurations investigated the simulated sting was adjusted up or down to accommodate the height of the current standoff. Model blockage corrections and jet boundary corrections were applied in the same manner to both full span and semi-span configurations. A flow angularity correction was also applied to both configurations (0.141° up flow for the full span model and 0.081° down flow for the semi-span model). The wind tunnel boundary layer removal system (BLRS) was used for all semi-span data presented in this paper unless otherwise noted. The use of the BLRS reduced the boundary layer on the floor of the wind tunnel from 10 inches to 2 inches at the moment reference center of the model. Surface flow visualization images were obtained of the wind tunnel floor around the semi-span configuration using an oil based mixture consisting of mineral oil, oleic acid, and titanium dioxide. Flow visualization images were obtained of the upper surface of the wing for both full span and semi-span configurations using fluorescent mini-tufts, ultraviolet strobe lights, and a video imaging system.

Discussion

Standoff Height Effects

One of the primary goals of this investigation was to determine the effects of variations in standoff height. The first step in this process was to look at height variation using a two-dimensionally shaped standoff. In order to do this the semi-span configuration was tested with no standoff, a 2-inch standoff, and a 6.4-inch standoff. The no-standoff configuration was chosen as the obvious case to represent the minimum standoff height. The 2-inch height, which was equal to approximately 30 percent of the fuselage radius, was chosen because it corresponds to the height of the floor boundary layer at the model moment reference center with the BLRS on. The 6.4-inch height, which was equal to approximately 93 percent of the fuselage raduis, was chosen because it compared to a standoff height which was investigated on a smaller scale EET model in another facility. It was further believed that the 6.4-inch height represented a reasonable maximum height and that a 2-D standoff any taller would produce no benefit. This standoff height is equivalent to about 3 times the floor boundary layer thickness with the BLRS on and was expected to result in large effects. The results obtained from these configurations are presented together for comparison in figure 5. The force and moment data indicate that for angles of attack up to 12° the configuration with the 2-inch standoff correlates better with full span data in terms of lift, lift-curve slope, and drag coefficient than the other standoff configurations. The no-standoff configuration results in a reduced lift-curve slope and a substantial drag

increase, whereas the larger standoff indicates an increase in lift-curve slope and a drag increase. Collectively these data indicate that increases in 2-D standoff height produce increases in lift-curve slope. The 2-inch standoff configuration however, produces a stall angle of attack that is approximately 4° less than that of the full span configuration. It is also noted that the no-standoff configuration comes closest to matching the stall angle of attack while the other configurations stall early. None of the standoff configurations produced a very good correlation with the full span configuration in terms of pitching moment. For the non-zero standoff configurations this could be due to a slight misalignment between the fuselage and standoff caused by balance deflections.

Pressure data presented for the inboard portion of the wing (figure 5(b)) indicate that at 16° angle-of-attack flow conditions on the slat and the leading edge of the main element correlate better with the full span data for the 2-inch standoff configuration than the other two standoff configurations. In fact, a trend is indicated which shows a flow acceleration over the slat and the main element leading edge as standoff height is increased. This could lead to the conclusion that increases in standoff height produce increases in the flow acceleration around the fuselage, which in turn produce the flow accelerations noted on the wing leading edge. When fuselage pressure data are compared for the various standoff configurations (figure 5(c)), it is shown that increases in standoff height do indeed produce increases in the flow acceleration around the fuselage. These data also further support the conclusion that the 2-inch standoff configuration more accurately simulates the full span configuration than the other standoff geometries.

Two additional standoff configurations were also tested as a part of this investigation, a three-dimensionally shaped 6.4-inch standoff which was a mirror image of the semi-fuselage, and a complete right side of the fuselage. It was anticipated that the size, which would offset the model farther from the tunnel floor, along with the 3-D shaping of these standoffs may act to reduce the effects of the floor boundary layer on the semi-span configurations. Force and moment data obtained for these additional standoff configurations are presented in figure 6. Lift losses and drag increases are noted for both configurations when compared to the full span data. More specifically, the 6.4-inch, 3-D standoff shows no improvement over the 6.4-inch, 2-D standoff, and the configuration with the complete fuselage produces the largest lift deficit and largest drag increase of all standoffs investigated. Even though the configuration with the complete fuselage shows good correlation with full span data in terms of pitching moment, the poor lift and drag correlation are still viewed as substantial drawbacks. Since these larger, mirror-image standoffs did not result in an overall improvement in correlation with full span data they were given no further consideration. Based on all the semi-span data presented thus far, the overall results indicate that semi-span configuration aerodynamics are quite sensitive to variations in standoff height.

Boundary Layer Height Effects

Another primary goal of the investigation was to determine the effects of variations in floor boundary layer height. In order to do this data were obtained with the tunnel boundary layer removal system (BLRS) off, which results in a 10-inch boundary layer at the model moment reference center, and with the BLRS on, which results in a 2-inch boundary layer. Longitudinal force and moment data are presented in figure 7(a) for the 2-inch, 2-D standoff configuration with the BLRS both off and on. These data indicate that the height of the floor boundary layer has little influence on the lift or drag coefficient data. This implies that the configuration aerodynamics is dominated by the wing and the flow over the fuselage has only a small influence. However, pitching-moment data indicate more sensitivity to flow over the fuselage as a positive increment in C_M is shown for the thinner floor boundary layer (BLRS on). Although not presented, very similar trends were also noted in the longitudinal data for the other standoff configurations. This result was somewhat surprising in that a thinner floor boundary layer was fully expected to produce more desirable results than a thicker one. Further analysis of the effects of the height of the floor boundary layer was conducted by obtaining total pressure measurements from two boundary layer rakes mounted on the fuselage as noted in figure 1. Data from these rakes are presented in the form of u/u_∞ in figures 7(b) and 7(c). The fuselage boundary layer rake data were obtained with the tangential blowing system (see fig. 4) in operation; however, this should not effect the trends indicated when comparing BLRS off and on. These data indicate that the use of the BLRS, and thus a thinner floor boundary layer, results in a semi-span fuselage boundary layer profile that more closely resembles the full span fuselage boundary layer profile. When the larger 10 inch boundary layer exists on the tunnel floor a substantial deceleration of the flow results on the semi-span fuselage. Therefore, a thinner floor boundary layer will promote a semi-span fuselage boundary layer that more accurately correlates with the full span fuselage

boundary layer. The investigation of the effects of standoff height and floor boundary layer height reveal that both parameters influence the flow over the semi-span configuration; however, the effects of variation in standoff height (from zero to approximately 100 percent of the fuselage radius) has a large effect on lift-curve slope and stall characteristics.

Undercut Standoff Leading Edge Effects

When any 2-D standoff is used, it is understood that a stagnation point will exist at some location on the leading edge. This stagnation point causes the free-stream flow to roll up on itself in the floor boundary layer, and a horseshoe vortex will form around the standoff leading edge. In order to document and illustrate this flow condition, a surface oil flow pattern was obtained on the tunnel floor for the 2-inch, 2-D standoff configuration. This oil flow pattern, presented in figure 8 for an angle of attack of 19°, gives an indication of the horseshoe vortex size and location.

It was anticipated that the presence of a horseshoe vortex around the leading edge of a 2-D standoff was detrimental to efforts to match the flowfield around a full span configuration. With this thought in mind two undercut leading edges as illustrated in figure 3(b) were tested on the 2-inch standoff. These undercut shapes are referred to as an S-curve leading edge and a parabola leading edge. The S-curve leading edge was designed using computational methods such that a favorable pressure distribution would result in the cockpit region of the forebody. The parabola leading edge was designed such that no forward facing surfaces would exist thereby resulting in a geometry which would make it much more difficult for a horseshoe vortex to form. Longitudinal force and moment data illustrating the effects of the standoff undercut leading edges are presented in figure 9(a). These data indicate that undercut standoff leading edges have essentially no effect on lift curve slope, but have a significant effect on the stall angle of attack. The S-curve leading edge increases the stall angle of attack by approximately 2° over the 2-D configuration, and the parabola leading edge increases the stall angle of attack by approximately 3°. These results thereby suggest that the elimination or reduction in size of the horseshoe vortex will improve correlation of semi-span and full span data in the region of maximum lift coefficient. This point is further supported upon reexamination of the lift coefficient data presented for the no-standoff configuration in figure 5(a). Even though the no-standoff configuration does not correlate well with full span data across the angle-of-attack range, it does match the stall angle of attack much better than the other 2-D standoff configurations. This may well be due to the fact that it is much more difficult for a horseshoe vortex to form on the no-standoff configuration.

Even though the undercut standoff leading edges do improve correlation of stall angle of attack and maximum lift coefficient with full span data, they are not without shortcomings. The undercut leading edges result in an increase in drag as compared to the 2-D leading edge, and the reason for this unfavorable characteristic is unknown. As a result a more thorough understanding of the flow physics will be pursued through computational and experimental efforts. Examination of the pitching-moment data reveals a nose-down increment beyond the stall angle of attack for all of the semi-span configurations. This indicates that wing stall begins on the inboard portion of the wing. This does not match the post stall nose-up increment indicated by the full span data. This inconsistency has also been noted in previous research[6]. The fact that the stall behavior on the semi-span configurations with undercut standoff leading edges does not match that on the full span model indicates that the influence of the floor boundary layer on the flowfield over the wing may still not be fully eliminated. Inboard wing pressure data are presented for an angle of attack of 19° in figure 9(b) to further illustrate the effects of the undercut standoff leading edges. These data indicate that the configuration with the 2-D standoff leading edge is producing less lift on the slat and main element than the undercut standoff configurations, while the data from the undercut configurations match the full span data relatively well. These data further support the inboard wing stall noted in the discussion of the pitching-moment data.

Further insight into the flow conditions on the wing upper surface was obtained through the use of flow visualization. Fluorescent mini-tuft images of the wing upper surface have been obtained for configurations with the 2-D standoff leading edge and the S-curve leading edge, and these images are presented for an angle of attack of 19° in figure 10. A region of separated flow is indicated inboard on the wing for the configuration with the 2-D standoff leading edge (fig. 10(a)), as would generally be expected due to the wing pressure data presented in the previous figure. The image of the wing for the configuration with the S-curve leading edge (fig. 10(b)) indicates smooth, attached flow over the entire inboard portion of the wing. These results suggest that the horseshoe vortex which forms around the leading edge of the 2-D standoff produces an undesirable flow disturbance which ultimately affects

the flow over the inboard portion of the wing. This disturbance promotes an inboard wing stall and resulting nose-down pitching moment. The undercut leading edge configurations ultimately stall in the same fashion; however, the leading-edge undercut shaping appears to be effective in delaying the onset of the flow disturbances which produce the inboard wing stall.

Tangential Blowing Effects

Another technique investigated to improve correlation of semi-span data with full span data was the use of tangential blowing in the juncture between the standoff and the floor. Tangential blowing reenergizes the floor boundary layer which in turn should reduce the effects of the floor boundary layer on the flowfield over the semi-span model. This blowing technique evolved from the successful use of juncture blowing to eliminate tunnel sidewall boundary layer separation for 2-D, high-lift airfoil testing[9]. In addition, computational efforts have also shown promising results using active boundary layer control concepts[7]. Ten blowing jets were located in the juncture between the standoff and the floor as illustrated in figure 4. Results were obtained for the 2-inch standoff with the 2-D leading

metric fuselage and the non-metric standoff. Any freestream flow that could be allowed to enter the region between these two parts may well impose an inappropriate loading on the internal centerline surface of the fuselage. In order to gain insight into the sensitivity of the semi-span configuration to seal design, two seal concepts were tested. One concept, referred to as the perimeter seal, consisted of a foam seal which ran longitudinally around the upper and lower surfaces of the fuselage and, as the name suggests, followed the perimeter of the fuselage. This seal was used on all of the configurations presented thus far. The other concept, referred to as the keel dam seal, was a simplified concept which consisted of a strip of foam attached to the model right on the fuselage centerline and extending the entire length of the fuselage. The foam seal was 0.75 inches wide and was attached to the fuselage for both concepts so that it just filled the gap between the fuselage and standoff without transferring a load between the two parts. Longitudinal force and moment data are presented in figure 12 for both seal concepts as installed on the 2-inch, 2-D standoff configuration. For angles of attack up to 16° the configuration with the keel dam seal produces a lift loss and a drag increase as compared to the perimeter seal

2. Configurations with no standoff produced a reduction in lift-curve slope and more drag than the baseline full span configuration.

3. Configurations with standoff heights on the order of the fuselage radius produced an increase in lift-curve slope and drag compared to the baseline full span configuration.

4. A 2-inch standoff, which was equal to approximately 30 percent of the fuselage radius, produced the best correlation with full span data for angles of attack below 12° of all the standoff configurations tested.

5. A 2-D standoff leading edge promotes the formation of a horseshoe vortex in the standoff/floor juncture and in turn promotes an early inboard wing stall.

6. The early inboard wing stall that occurred with the 2-D, 2-inch standoff was effectively delayed by an undercut standoff leading edge.

7. Tangential blowing in the standoff/floor juncture also proved to be an effective technique to alleviate the early inboard wing stall that occurred with the 2-D leading edge on the 2-inch standoff.

8. Semi-span model aerodynamics were found to be quite sensitive to variations in the design of the seal between the fuselage and standoff. Care should be taken to ensure that this region is sealed effectively.

References

1. Lynch, F. T.: Experimental Necessities for Subsonic Transport Configuration Development. AIAA Paper 92-0158, January 1992.

2. Viehweger, G.; and Ewald, B.: Half Model Testing in the Cologne Cryogenic Tunnel (KKK). AIAA Paper 94-2511, June 1994.

3. Milholen II, W. E.; and Chokani, N.: Effect of Sidewall Boundary Layer on Transonic Flow Over a Wing. *Journal of Aircraft*, Vol. 31, July 1994, pp. 986-988.

4. Franz, H. P.: The Half-Model Technique in the Wind Tunnel and its Employment in the Development of the Airbus Family. NASA TM-76970, August 1982. Translation of DGLR Paper 81-118.

5. Boersen, S. J.: Half-Model Testing in the NLR High-Speed Wind Tunnel HST, A 1981 Status Report. NLR TR 82123U, August 1982.

6. Earnshaw, P. B.; Green, A. R.; Hardy, B. C.; and Jelly, A. H.: A Study of the use of Half-Models in High-Lift Wind-Tunnel Testing. AGARD-CP-515, October 1992, pp. 20.1–20.9.

7. Milholen II, W. E.; Chokani, N.; and McGhee, R. J.: Development of Semi-span Model Test Techniques. AIAA Paper 96-2412, June 1996.

8. Gentry, Garl L., Jr.; Quinto, P. Frank; Gatlin, Gregory M.; and Applin, Zachary T.: The Langley 14- by 22-Foot Subsonic Tunnel: Description, Flow Characteristics, and Guide for Users. NASA TP-3008, September 1990.

9. Paschal, K., Goodman, W., McGhee, R., Walker, B., and Wilcox, P. A.: Evaluation of Tunnel Sidewall Boundary-Layer-Control Systems for High-Lift Airfoil Testing. AIAA Paper 91-3243, September 1991.

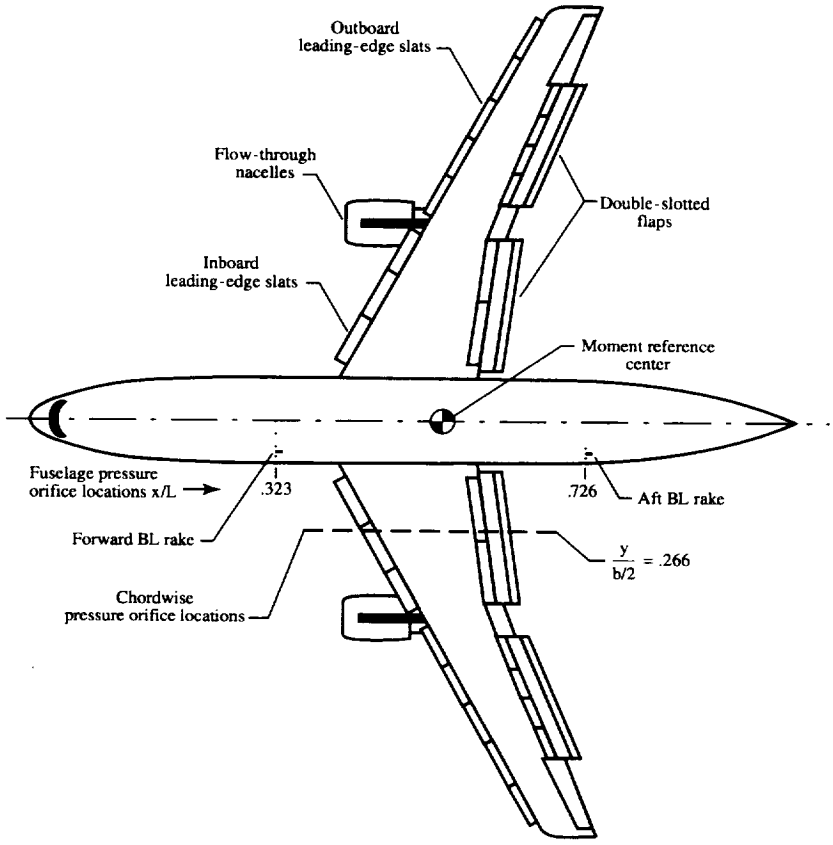

Figure 1. Full span Energy Efficient Transport (EET) model in the take-off configuration.

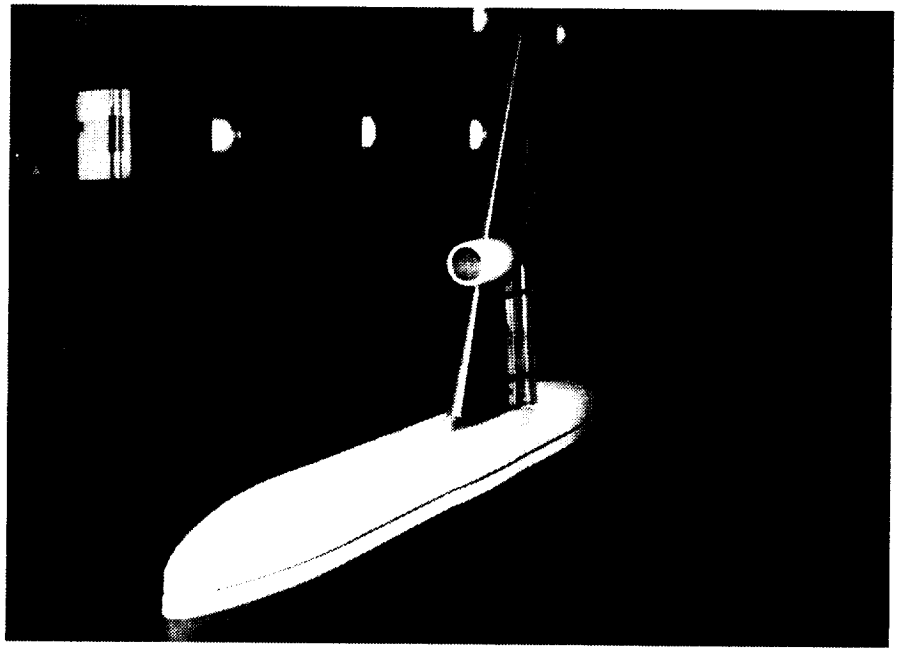

Figure 2. Semi-span EET model as tested with the 2-inch, 2-D standoff in the 14- by 22-Foot Subsonic Tunnel.

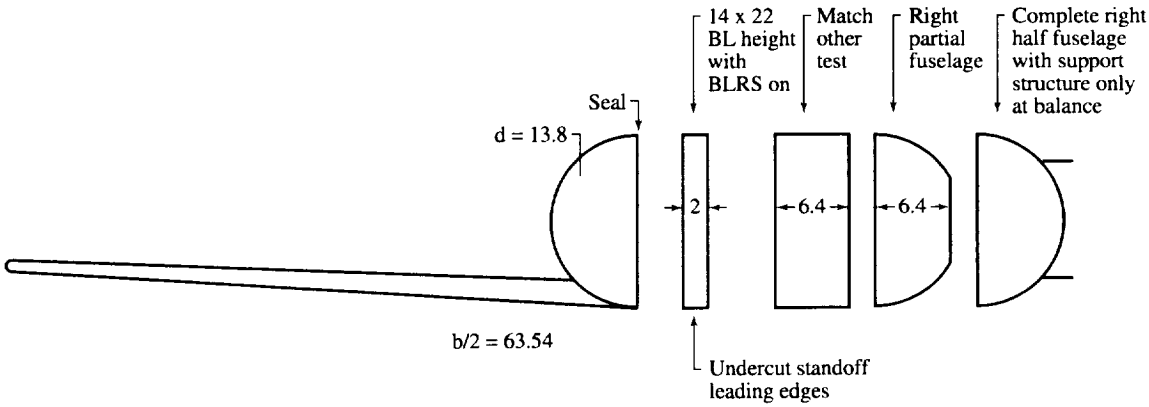

(a) Cross-sectional views of the standoff geometries.

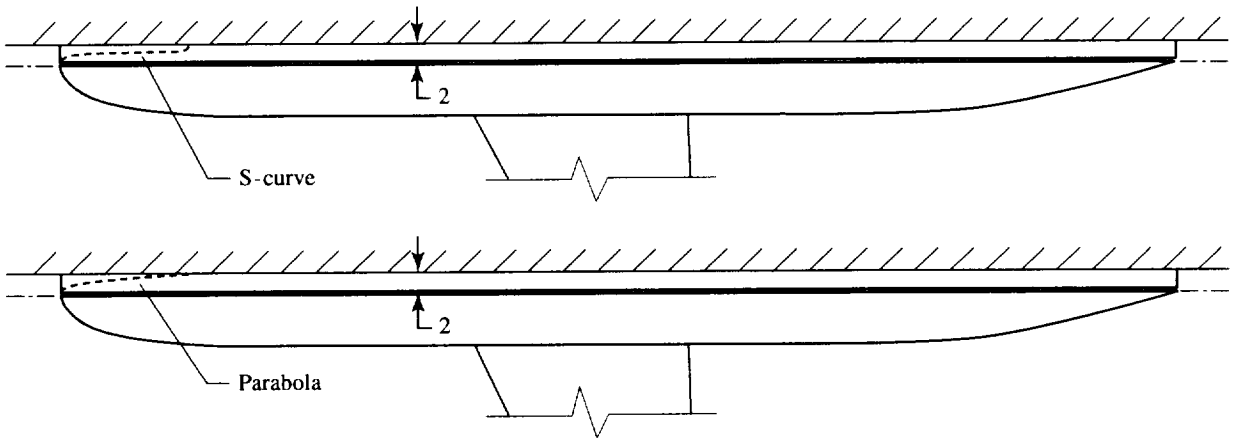

(b) Top-view illustrations of the undercut leading edges tested on the 2-inch standoff.

Figure 3. Standoff geometries tested on the semi-span model. All dimensions are in inches.

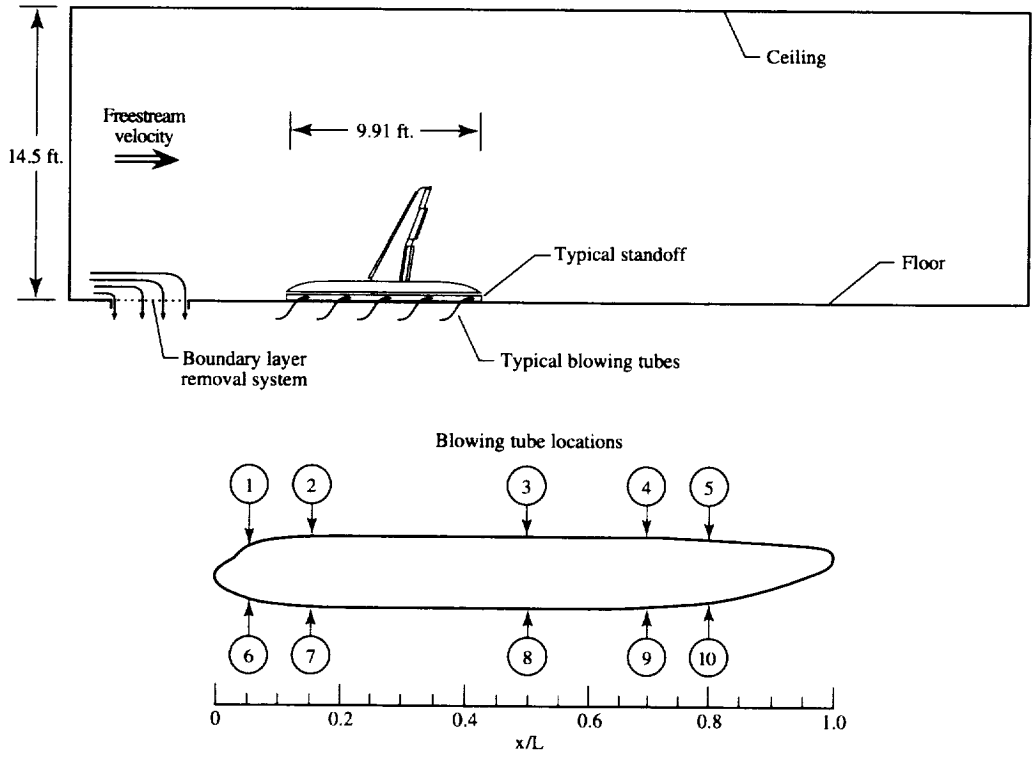

Figure 4. Sketches illustrating the tangential blowing test setup.

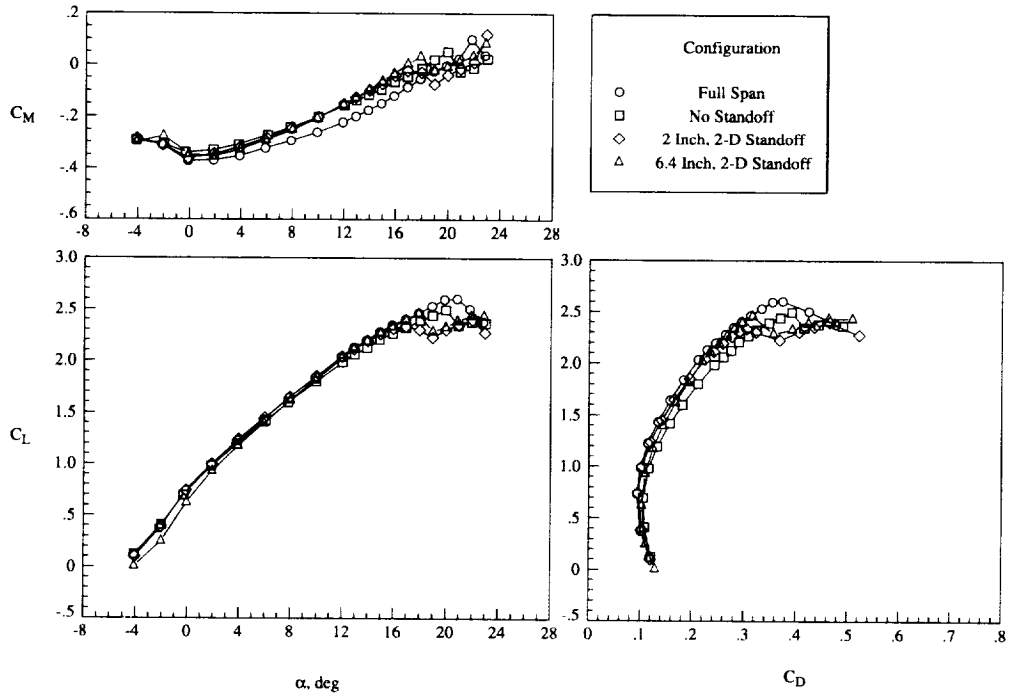

(a) Longitudinal force and moment data.

Figure 5. Data illustrating the effects of variations in 2-D standoff height.

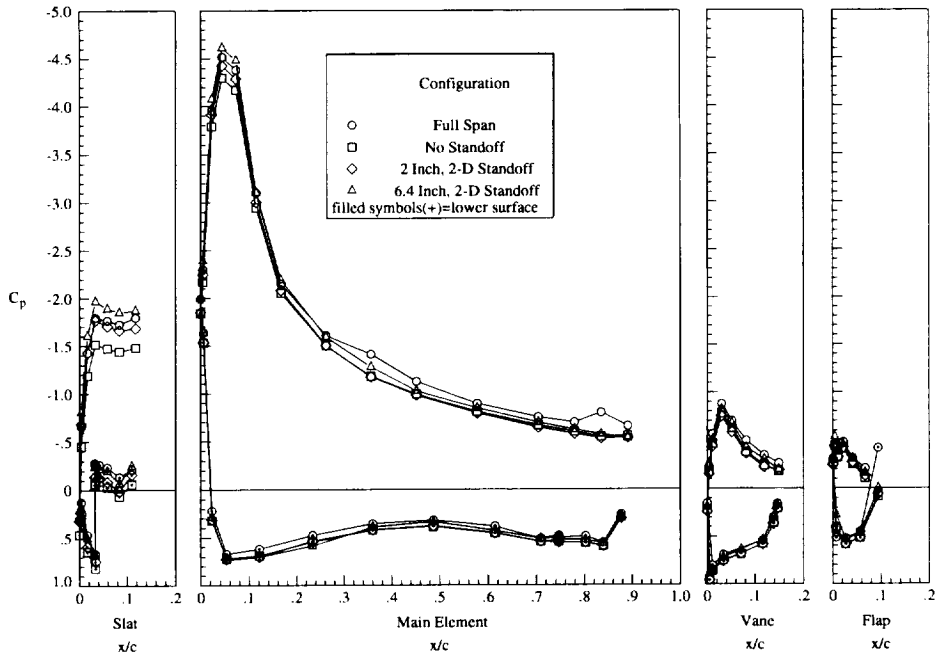

(b) Wing pressure data. $\alpha = 16^{o}$.

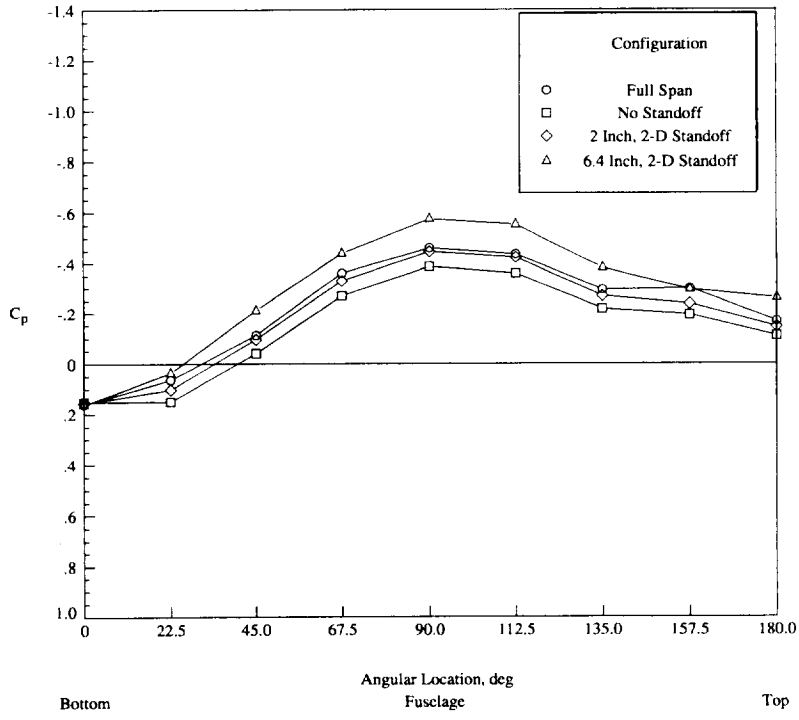

(c) Comparison of full span and semi-span fuselage pressure data. $x/l = 0.323$, $\alpha = 16^{o}$.

Figure 5. Concluded.

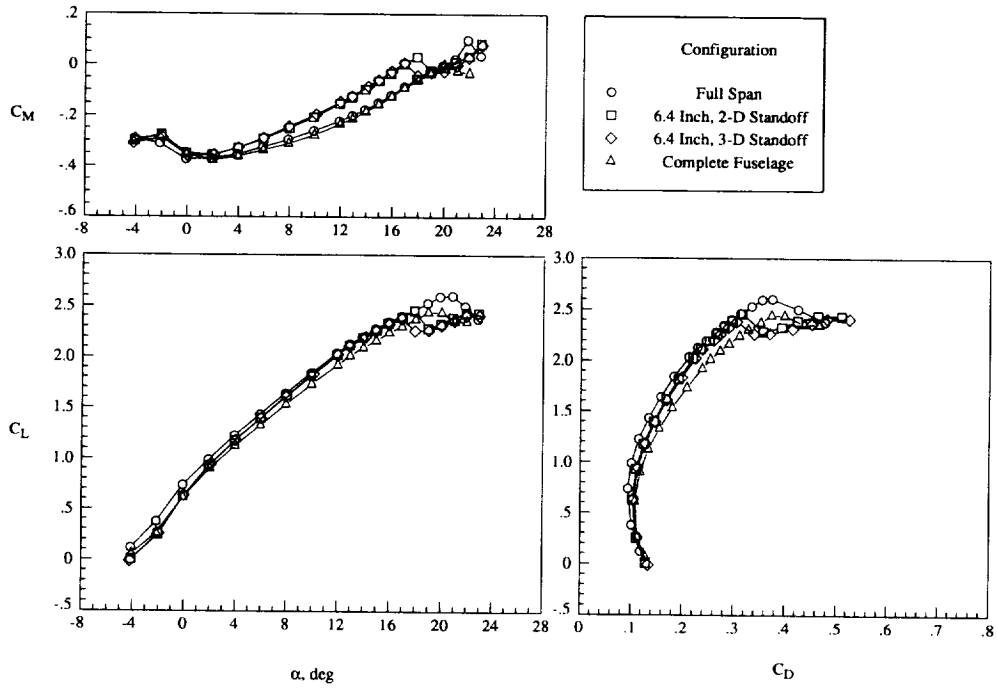

Figure 6. Longitudinal force and moment data illustrating the effects of the larger, mirror-image standoffs.

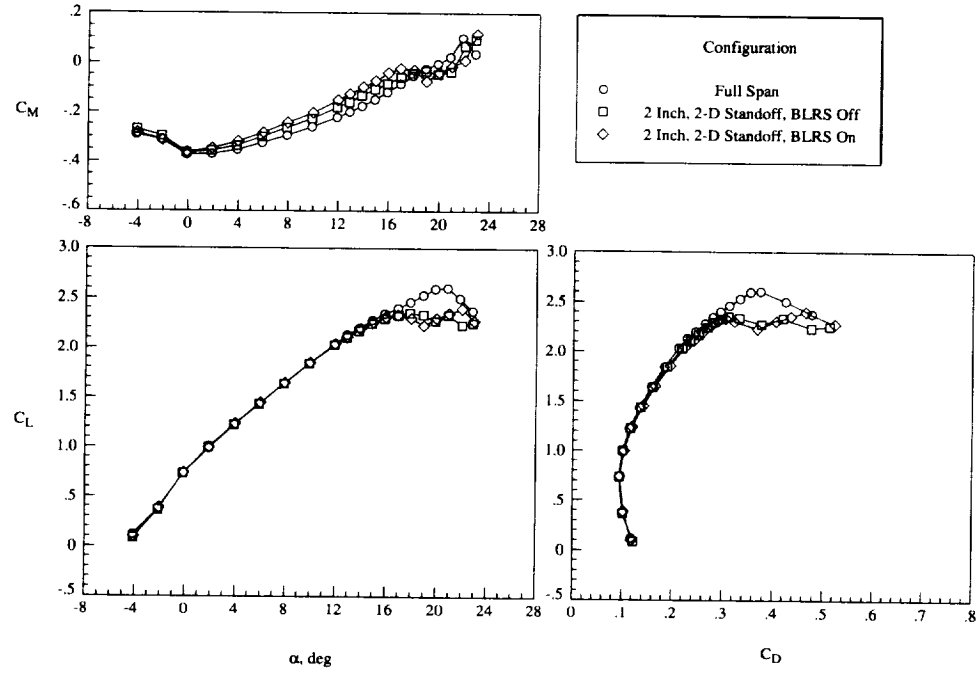

(a) Longitudinal force and moment data.

Figure 7. Data illustrating the effects of variations in tunnel floor boundary layer height.

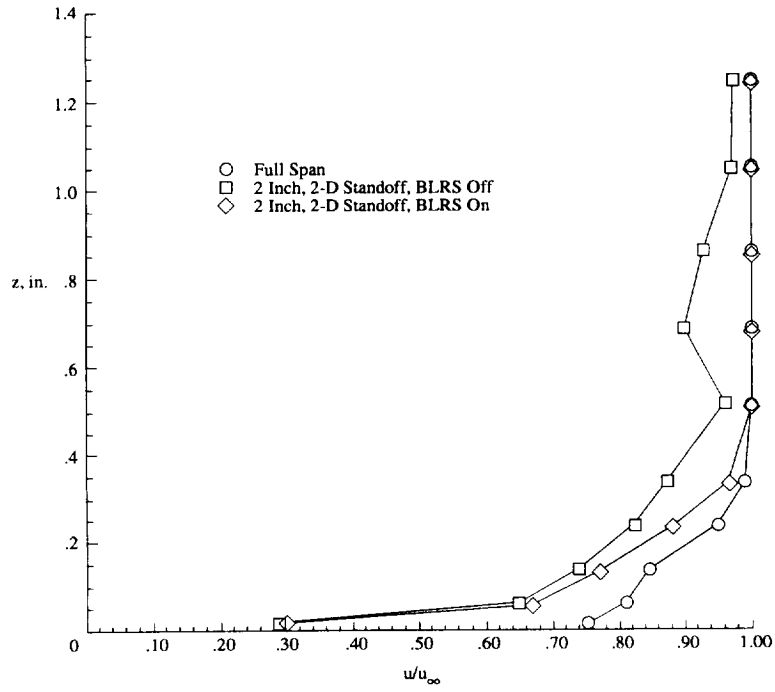

b) Fuselage boundary layer rake data from forward rake. $C_\mu = 0.003$, $\alpha = 8^o$.

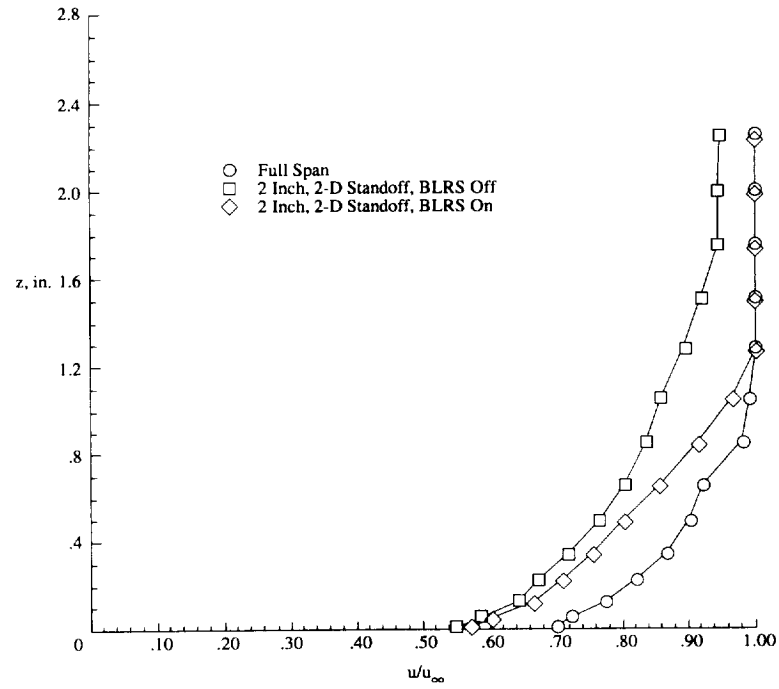

c) Fuselage boundary layer rake data from aft rake. $C_\mu = 0.003$, $\alpha = 8^o$.

Figure 7. Concluded

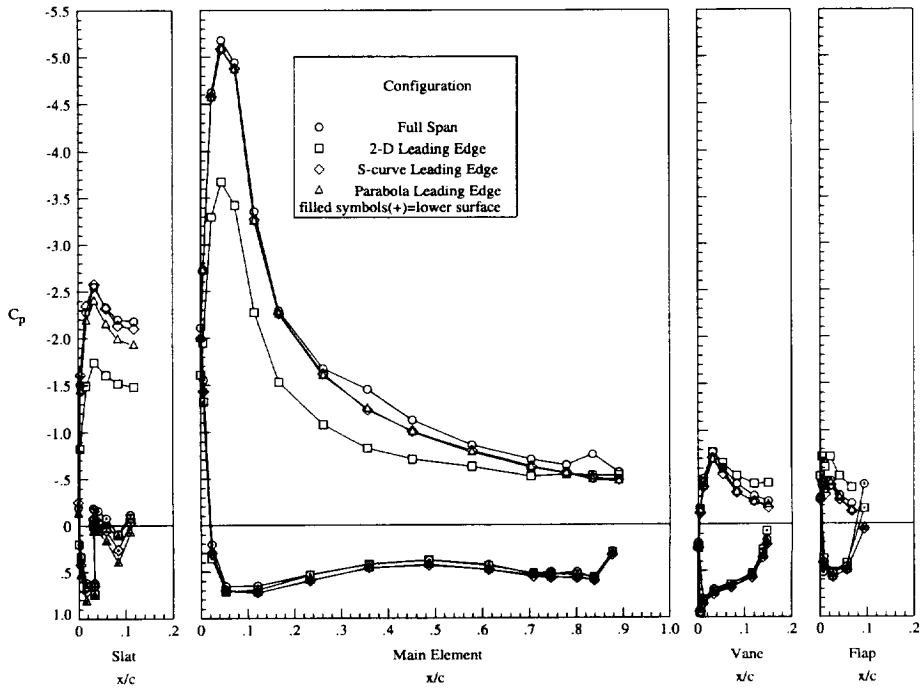

(b) Wing pressure data. $\alpha = 19^{o}$.

Figure 9. Concluded.

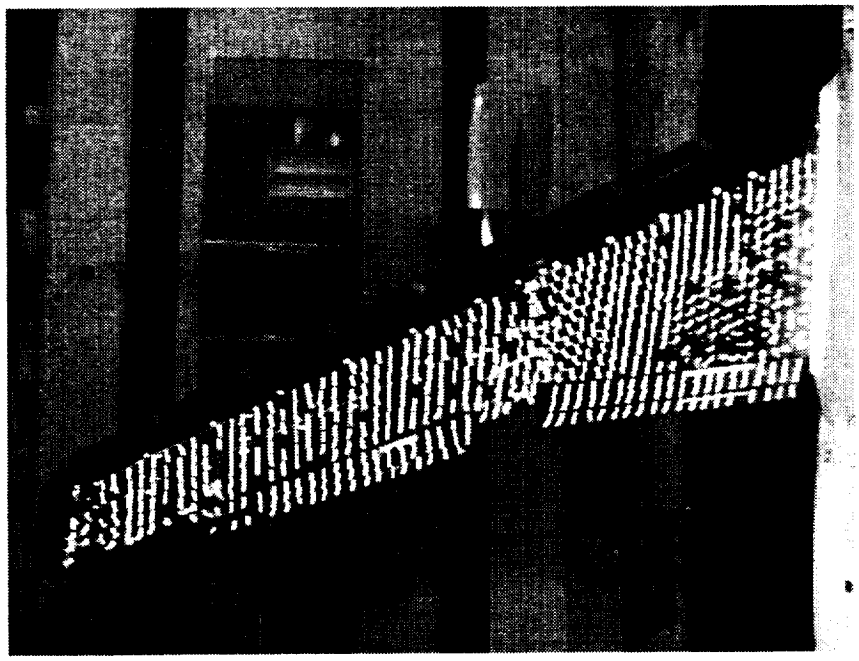

(a) 2-D standoff leading edge.

Figure 10. Flow visualization illustrating wing upper surface flow characteristics with 2-inch standoff. $\alpha = 19^{o}$.

(b) S-curve standoff leading edge.

Figure 10. Concluded.

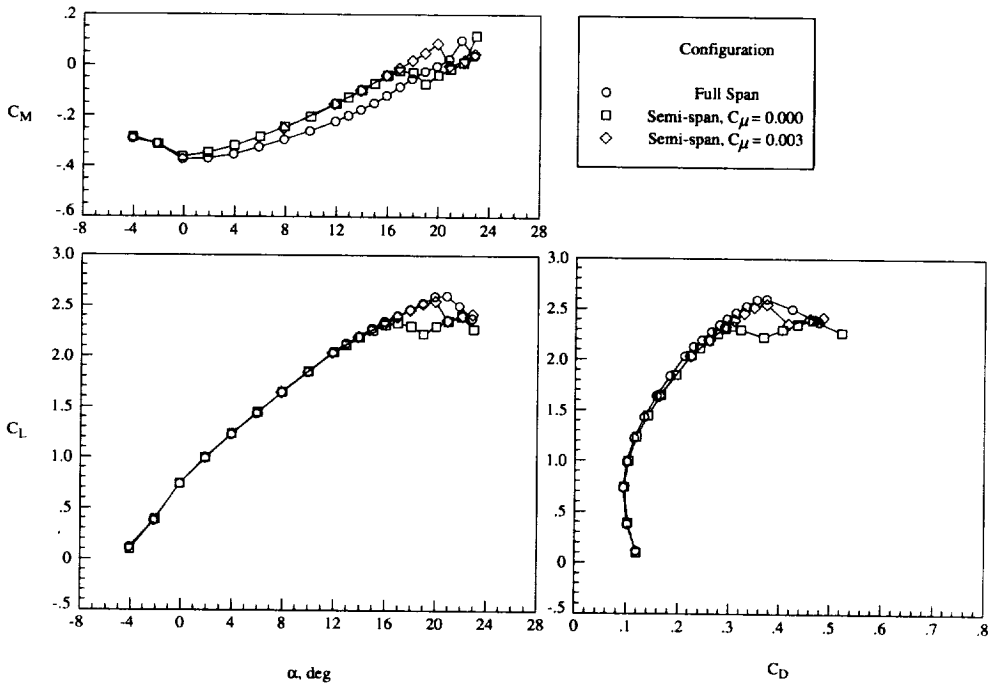

(a) Longitudinal force and moment data.

Figure 11. Data illustrating the effects of tangential blowing in the standoff/floor juncture. 2-inch, 2-D standoff configuration.

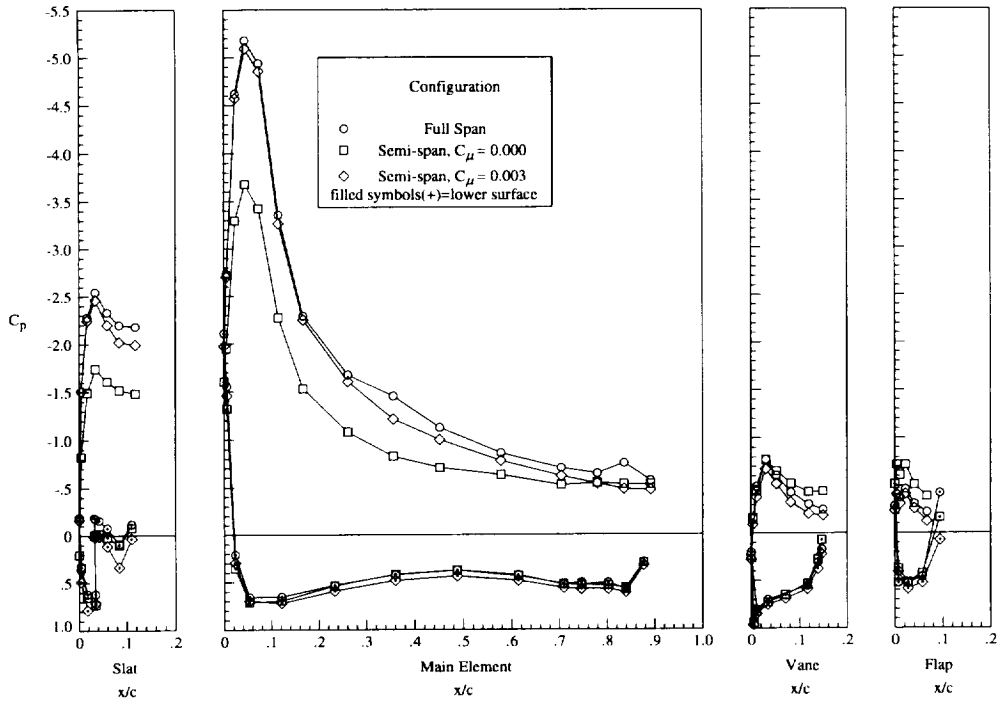

(b) Wing pressure data. $\alpha = 19^o$.

Figure 11. Concluded.

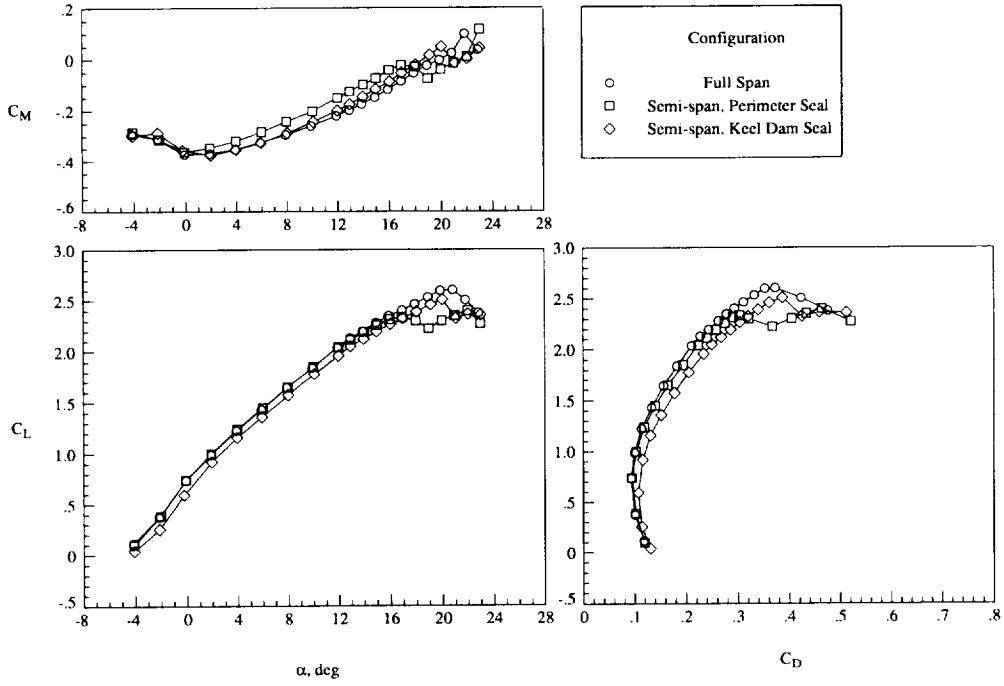

Figure 12. Longitudinal data illustrating the sensitivity to variations in the fuselage/standoff seal design. 2-inch, 2-D standoff configuration.